

Article

Preparation of Poly(Butadiene–Styrene–Vinyl Pyridine)/Poly(Acrylonitrile–Butadiene) Core–Shell Nanoparticles by Intermittent Seeded Emulsion Polymerization and Their Catalytic Latex Hydrogenation

Fei Yuan ¹, Xudong Li ¹, Jianying Dou ¹, Baojia Zhang ¹, Xueling Song ², Lin Li ¹, Junjie Liu ¹, Yanyan Li ¹, Yigao Jiang ³ and Hui Wang ^{1,*} 

¹ School of Polymer Science and Engineering, College of Chemistry and Molecular Engineering, College of Economics and Management, Qingdao University of Science and Technology, Qingdao 266042, China; yf734982036@163.com (F.Y.); qustgfzlx@126.com (X.L.); 13864338873@163.com (J.D.); zhangbaojia2004@163.com (B.Z.); qustlilin@hotmail.com (L.L.); junjie0536@163.com (J.L.); liyanyan6771@163.com (Y.L.)

² School of Materials and Chemistry, University of Shanghai for Science and Technology, Shanghai 200093, China; happy_shirlene@163.com

³ Yangzhou High-Tech Rubber & Plastic Limited Company, Yangzhou 225124, China; yzgxss@yzgxss.com

* Correspondence: hwang@qust.edu.cn

Abstract: Seed emulsion polymerization was an effective modification method to improve not only the properties of polymers but also the compatibility between different polymers by designing special core-shell structures. In this study, poly (butadiene-styrene-vinyl pyridine) (VPR)/poly (acrylonitrile-butadiene) (NBR) core-shell nanoparticles (VPR/NBR) were prepared by seed emulsion polymerization using VPR as seed emulsion and butadiene and acrylonitrile as monomers. Subsequently, HVPR/HNBR was obtained by direct hydrogenation of the core-shell nanoparticles in latex using Wilkinson's catalyst under high temperature and H₂ pressure. It is noteworthy that the unsaturated C=C double bonds in the core (VPR) and shell (NBR) of HVPR/HNBR nanoparticles were reduced simultaneously during the hydrogenation process without obvious sequence. The particle size and size distribution of the particles remained consistent before and after hydrogenation, indicating that the synthesized core-shell nanoparticles have excellent stability. This study provides a new perspective on the chemical modification of NBR and promises an environmentally friendly "green" process for the industrial hydrogenation of unsaturated elastomers.

Keywords: core-shell nanoparticles; seed emulsion polymerization; catalytic latex hydrogenation; particle size; latex stability



Citation: Yuan, F.; Li, X.; Dou, J.; Zhang, B.; Song, X.; Li, L.; Liu, J.; Li, Y.; Jiang, Y.; Wang, H. Preparation of Poly(Butadiene–Styrene–Vinyl Pyridine)/Poly(Acrylonitrile–Butadiene) Core–Shell Nanoparticles by Intermittent Seeded Emulsion Polymerization and Their Catalytic Latex Hydrogenation. *Catalysts* **2024**, *14*, 277. <https://doi.org/10.3390/catal14040277>

Academic Editor: Salah-Eddine Stiriba

Received: 5 March 2024

Revised: 16 April 2024

Accepted: 16 April 2024

Published: 19 April 2024



Copyright: © 2024 by the authors. Licensee MDPI, Basel, Switzerland. This article is an open access article distributed under the terms and conditions of the Creative Commons Attribution (CC BY) license (<https://creativecommons.org/licenses/by/4.0/>).

1. Introduction

The synthesis of nanoscale particulate latexes by emulsion polymerization or copolymerization has attracted much attention in various research fields and has been widely applied [1–3]. Emulsion polymerization is favored for its ability to effectively mitigate the heat generated during polymerization, reduce system viscosity at high conversion rates, and precisely control the reaction extent and nanoparticle size. It is recognized that emulsion polymerization can be categorized into intermittent, semi-continuous, and continuous processes based on different feeding methodologies [4]. Over the past few decades, several innovative emulsion polymerization techniques have emerged, including seeded emulsion polymerization, soap-free emulsion polymerization, and reverse-phase emulsion polymerization, among others. Notably, seeded emulsion polymerization has proven to be an effective method for chemical modification [5–8].

Compared to latex obtained via conventional emulsion polymerization, latex prepared through seeded emulsion polymerization exhibits a uniform particle size distribution (PSD) and enhanced stability. Consequently, this method is widely employed in the synthesis of various latex products, especially rubber latex. In one instance, poly(methyl methacrylate)–poly(acrylonitrile–co–butadiene) (PMMA–NBR) core–shell nanoparticles were synthesized using a two-stage semibatch microemulsion polymerization approach [9]. PMMA, NBR, and Gemini surfactant 12–3–12 (GS 12–3–12) were employed as the core, shell, and emulsifier, respectively. It was observed that the continuous addition mode and the strong interfacial activity of GS 12–3–12 facilitated the formation of the core–shell structure. Furthermore, the concentration of GS 12–3–12 significantly influenced the particle size and morphology of the core–shell nanoparticles. In general, higher surfactant concentrations were conducive to synthesizing stable spherical emulsions.

Sheng X. [10] prepared core–shell nanoscale PBA–PMMA composite latex with high solid content using the microemulsion polymerization method. The results demonstrated that the highest solid phase content was achieved at a surfactant/monomer ratio of 5.25%. Both the surfactant and core monomer usage had substantial impacts on the final emulsion particle size. Furthermore, Mun H. [11] applied a reversible addition–fragmentation chain transfer (RAFT) polymerization method to produce SBR latex (ESBR) with a narrow molecular weight distribution. Comparative analysis with conventional SBR latex revealed that ESBR exhibited improvements in various physical properties, including wear resistance, mechanical properties, and dynamic viscoelastic properties.

The presence of C=C bonds in diene-based polymers (e.g., NBR, SBR, and VPR) has been known to compromise their chemical, physical, and mechanical properties leading to deterioration of the ageing properties of the materials, which are susceptible to oxidative and ozone decomposition in long-term use. Due to the high saturation of its molecular chains, hydrogenated elastomers have demonstrated exceptional stability in withstanding extreme environmental conditions and have found applications in various demanding industrial sectors, including automotive components, oil drilling, aerospace, and other performance-critical environments [12]. Consequently, hydrogenated nitrile rubber (HNBR) has emerged as a material that offers superior resistance to heat and aging while retaining its inherent oil resistance and wear resistance properties [13,14]. The primary challenge in producing hydrogenated nitrile rubber (HNBR) has been investigated to achieve selective hydrogenation of the C=C bonds while maintaining the integrity of the nitrile groups within the rubber [15,16].

The hydrogenation of unsaturated polymers can be divided into catalytic hydrogenation and non-catalytic hydrogenation processes. Diimide hydrogenation falls into the non-catalytic category. As a reducing agent, diamine can effectively reduce non-polar unsaturated bonds, while sparing polar unsaturated bonds. However, this hydrogenation process gives rise to numerous side reactions that significantly reduce hydrogenation efficiency and even promote polymer crosslinking, thereby impairing processability of the elastomer [17,18].

Currently, solution hydrogenation, an efficient catalytic hydrogenation process, has enabled the industrialization of the hydrogenation of diene polymers. Nevertheless, solution hydrogenation has some drawbacks, including limitations in achieving high degrees of hydrogenation (above 96%) [19–23] even at elevated temperatures and pressures, as well as substantial solvent consumption, leading to environmental concerns, increased costs, and complexity in the hydrogenation process [20].

To address these issues, the latex hydrogenation process has emerged as a promising alternative. It offers environmental benefits and integrates seamlessly with the emulsion polymerization system [22]. This approach is actively being pursued for commercialization by rubber industry partners and has become a prominent research area in academia. In particular, the catalyst system plays a crucial role in emulsion hydrogenation. Wang et al. prepared 95% high conversion HNBR latex using 0.1 wt% catalyst at 130 °C and 6.89 MPa

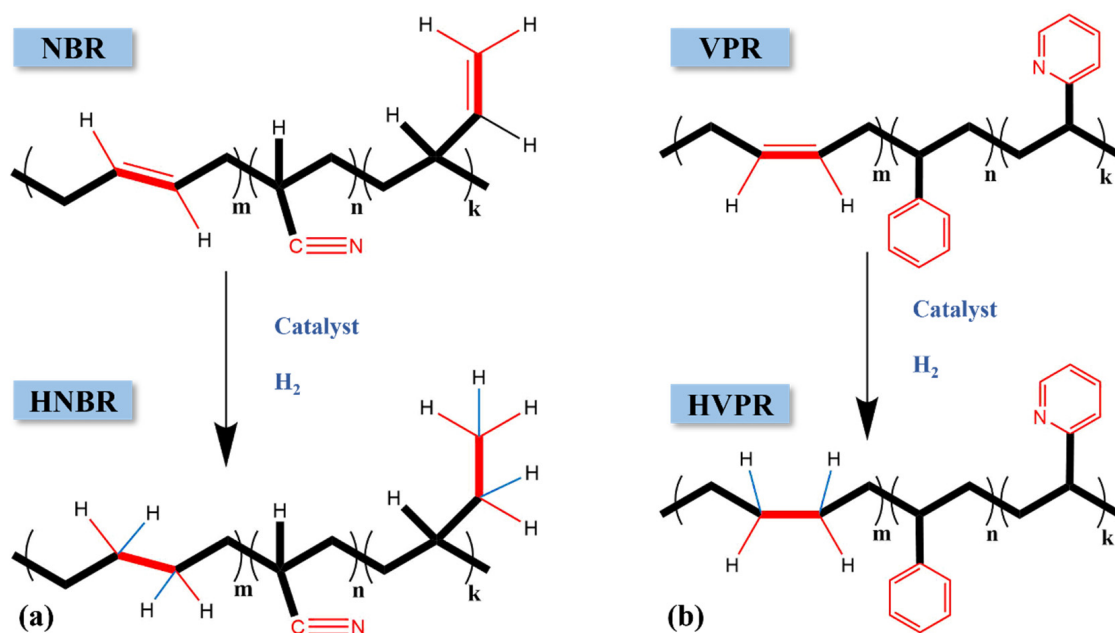
of H₂ without using any organic solvent. The hydrogenation rate was found to increase as the nanoparticle size decreased [24].

In our previous report, H. Wang [9] prepared core-shell latex nanoparticles, in which poly (methyl methacrylate) was used as the core and the shell was the NBR. The PMMA–NBR core-shell nanoparticles were then hydrogenated to PMMA–HNBR nanoparticles. In the above process, the NBR shell was hydrogenated completely, while PMMA was intact without any hydrogenation. The main reason was the absence of the C=C within the PMMA polymer chains. Furthermore, we were wondering about the hydrogenation phenomena for the core-shell nanoparticles with both core and shell having C=C bonds. VPR has excellent tensile and tear strengths. We chose VPR as the seed emulsion to give NBR excellent mechanical properties while maintaining its inherent heat and oil resistance.

In this study, we employed a seeded emulsion polymerization technique to fabricate poly (butadiene-styrene-vinyl pyridine)/poly (acrylonitrile-butadiene) latexes with varying core-to-shell mass ratios. Notably, the particle size of these latexes underwent significant changes throughout the seeded emulsion polymerization process. To elucidate the hydrogenation mechanism concerning the two distinct structural molecular chains present, we also investigated the hydrogenation sequence of these structures within the core-shell VPR/NBR polymer during the hydrogenation process.

2. Results

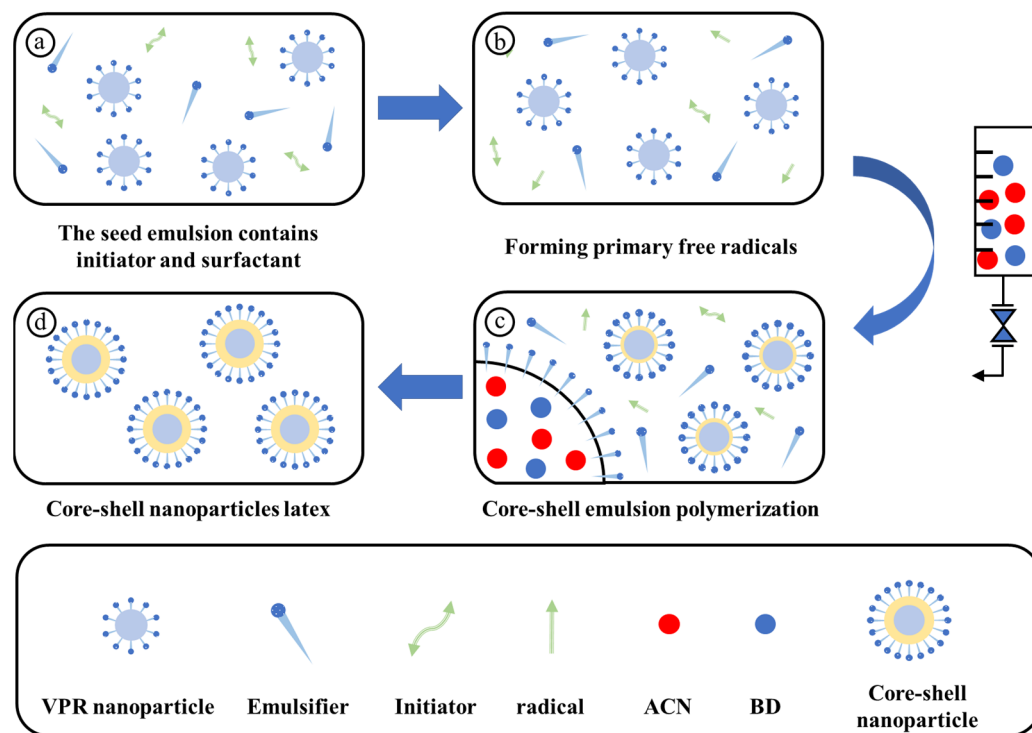
The molecular structures of the two polymers before and after hydrogenation were shown in Scheme 1. After hydrogenation, unsaturated C=C double bonds were all reduced to single bonds, while special groups such as cyano and pyridine rings remained untouched.



Scheme 1. The catalytic hydrogenation process of NBR (a) and VPR (b).

The typical synthesis process of nanoparticles via the seeded emulsion polymerization method is elucidated in Scheme 2. Seeded emulsion polymerization typically consists of two stages. In the first stage, seed latex of a specific size is prepared. In the second stage, monomers and initiators are introduced into the seed latex system, while the emulsifier concentration in the aqueous phase is rigorously controlled to prevent the formation of new particles, ensuring that the newly added monomers continue to polymerize on the existing “seeds”. The growth process of the particles during the second stage is outlined in Scheme 2. Initially, as shown in Scheme 2a, a specific quantity of initiator and emulsifier is added to the seed latex, where stirring and heating lead to the dispersion of the initiator

within the latex and its gradual decomposition into free radicals as polymerization proceeds (Scheme 2b) [25]. Subsequently, upon introduction into the reactor, the monomer becomes emulsified into monomer droplets, by diffusing from these droplets into the micelles continuously, ensuring a sufficient monomer concentration within the nanoparticles (Scheme 2c). Ultimately, nanoparticles with a core–shell structure are generated within the emulsion (Scheme 2d). It should be emphasized that this process of adding monomer to the latex should be strictly controlled with a slow and uniform flow rate of the monomer.

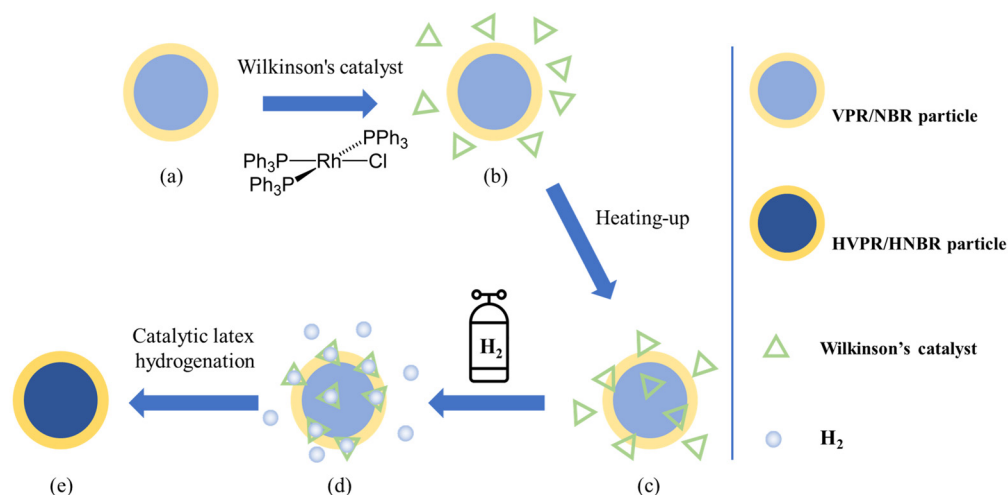


Scheme 2. Schematic diagram of nanoparticle synthesized by core–shell emulsion polymerization.

As the polymerization progressed, the available emulsifier became insufficient to effectively cover the expanding surface of the latex nanoparticles. Therefore, it was necessary to introduce additional surfactants into the reaction system to ensure the stability of the latex as the shell nanoparticles expanded. Initially, during the polymerization reaction, the small size of the seed latex could only accommodate the growth of a chain radical. Moreover, the protective role of the emulsifier on the micelle surface became increasingly critical as polymerization advanced, ensuring the longevity of the chain radical [26,27]. The polar negative group SO^{3-} in the SDS anionic surfactants could charge the particles, leading to more stable latex based on the electrostatic repulsion. Therefore, SDS was used in seed emulsion polymerization and latex hydrogenation experiments. To avoid the generation of gels at higher conversion rate, the solid content, time, and the conversion rate of the monomer polymerization were controlled at $30 \pm 2\%$, within 5 h, and about 80 wt%, respectively. These precautions were crucial for achieving stable polymerization processes.

Scheme 3 outlines the stages of catalytic latex hydrogenation of core–shell nanoparticles. The latex hydrogenation involves four key steps: (1) catalyst addition and uniform dispersion (a–b): The catalyst is added to the latex and uniformly dispersed throughout the nanomicelles with stirring in the system. (2) Catalyst Interaction with nanoparticles (b–c): Under stirring and heating, the catalyst molecules come into contact with the core–shell nanoparticles and penetrate to their interior. (3) Initiation of latex hydrogenation (c–d): The catalytic latex hydrogenation begins with the introduction of the targeted reaction temperature and hydrogen gas. (4) Mass transfer of hydrogen (d–e): The mass transfer process of H_2 from gas–liquid–solid is a key step in the hydrogenation of diene-based latex

nanoparticles. Stirring can greatly facilitate the movement of H_2 from the gas phase into the aqueous phase. The H_2 in the aqueous phase consists of two components: 1. H_2 present in the form of bubbles (which accounts for the major part); and 2. H_2 dissolved in water. H_2 in the aqueous phase diffuses into the interior of the nanoparticles through the surfactant layer, where it undergoes hydrogenation with the polymer in the presence of a catalyst. Finally, the hydrogenation product is generated. This description highlights the intricate steps involved in the catalytic latex hydrogenation process [28].



Scheme 3. Schematic diagram of the catalytic latex hydrogenation of VPR/NBR polymer nanoparticles.

2.1. Particle Size of Core–Shell Polymer Latex Nanoparticles

The properties of latex nanoparticles play a crucial role in determining the properties of core–shell latex, especially in the context of rubber materials. To confirm the success of the seeded emulsion polymerization, it is essential to examine the alteration in the number of nanoparticles before and after polymerization. Therefore, this discussion focuses on the variations in the number and average particle size of nanoparticles as the weight of the shell monomers (butadiene and acrylonitrile) increases. The stability of nanoparticles determines the properties of the material; therefore, the study of changes in nanoparticle properties is essential to assess the quality and effectiveness of the polymerization process.

Figure 1a illustrates a substantial increase in polymer particle size with the rising NBR weight at a constant polymerization temperature of 70 °C. Simultaneously, a gradual increase in the number of particles (N_p) in the latex was observed. Conversely, when the reaction temperature was increased from 40 to 70 °C (Figure 1b), there was an evident reduction in the particle size of latex particles accompanied by an increase in N_p . It was noteworthy that when the reaction temperature was further raised to 80 °C, the latex particle size decreased even further, while N_p increased. The reasons for these observations can be attributed to several factors. Firstly, the increase in the rate and concentration of radical generation at higher temperatures facilitates the diffusion of more radicals into the micelles, leading to the formation of newly generated nanoparticles. Secondly, elevated temperatures enhance the solubility of monomers in the aqueous phase, resulting in higher monomer concentration in this phase. Additionally, the heightened rate of chain propagation at elevated temperatures contributes to the production of more oligomeric chains in the aqueous phase [29]. Conversely, the increase in temperature to 80 °C may have adverse effects due to the following reasons: Firstly, it promotes the chain termination reaction and drastically shortens the radical lifetime. Secondly, the high polymerization rate in a high-temperature environment can trigger auto-acceleration, which weakens micelle stability to some extent and can even lead to nanoparticle disruption [30]. Hence, it is inferred that temperatures beyond a certain range might have detrimental effects on the emulsion. Understanding these temperature-related effects on latex particle size

and number is crucial for optimizing the emulsion polymerization process and achieving desired nanoparticle characteristics.

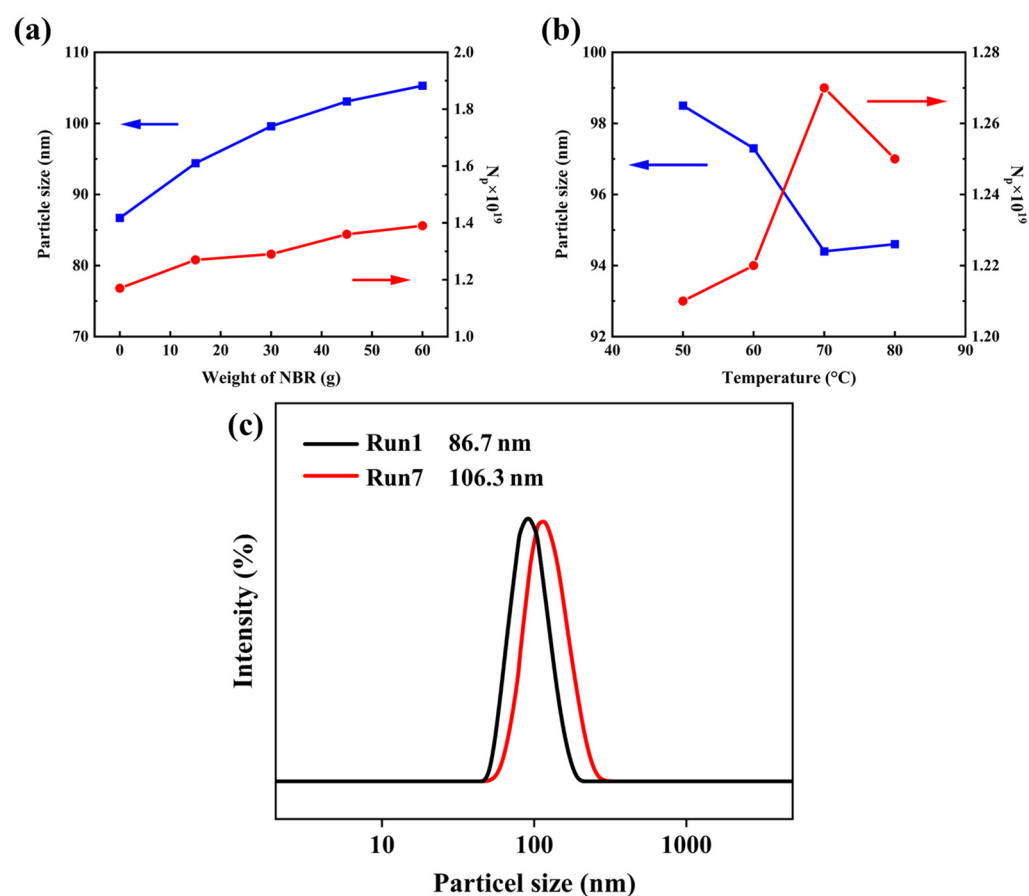


Figure 1. The effect curves of the NBR weight (a) and temperature (b) on particle size and N_p ; (c) particle size and particle size distributions of Run 1 (VPR) and Run 7 (VPR/NBR).

Dynamic light scattering (DLS) was employed to investigate the changes in latex particle size. Initially, the average particle size of VPR latex nanoparticles measured approximately 86.7 nm before the polymerization process. Subsequently, following the seeded emulsion polymerization (Figure 1c), this size increased to 106.3 nm. Importantly, the particle size distribution of nanoparticles in the latex remained narrow after polymerization, which indicates that the core-shell latex maintains the particle size uniformity of the nanoparticles. This DLS analysis provides valuable insights into the size variations of latex particles during the polymerization process, underscoring the ability to achieve consistent and controlled particle size uniformity in core-shell latex nanoparticles.

2.2. Morphology of Core-Shell Latex Nanoparticles

Seeded emulsion polymerization is a distinctive form of graft polymerization characterized by the growth of molecular chains on the surface of spherical nanoparticles, resulting in a special core-shell structure [7]. Transmission electron microscopy (TEM) images of VPR and NBR, displayed in Figure 2a,b, respectively, reveal a monolayer structure. Notably, as depicted in Figure 2c,d, the thickness of the outer layer of core-shell nanoparticles experienced a substantial increase owing to the greater weight of the shell polymer monomer. The microstructure analysis of HVPR/HNBR latex unveils a brighter TEM image post-hydrogenation when compared to its pre-hydrogenation state (Figure 2e,f). This phenomenon may be attributed to the reduced polarity of the molecular chain resulting from the reduction of C=C bonds. The specific alterations in the microstructure of core-shell nanoparticles during polymerization and hydrogenation are elucidated in Figure 2g [31].

These TEM images provide valuable insights into the structural transformations of core-shell nanoparticles throughout the polymerization and hydrogenation processes, further enhancing our understanding of these complex reactions.

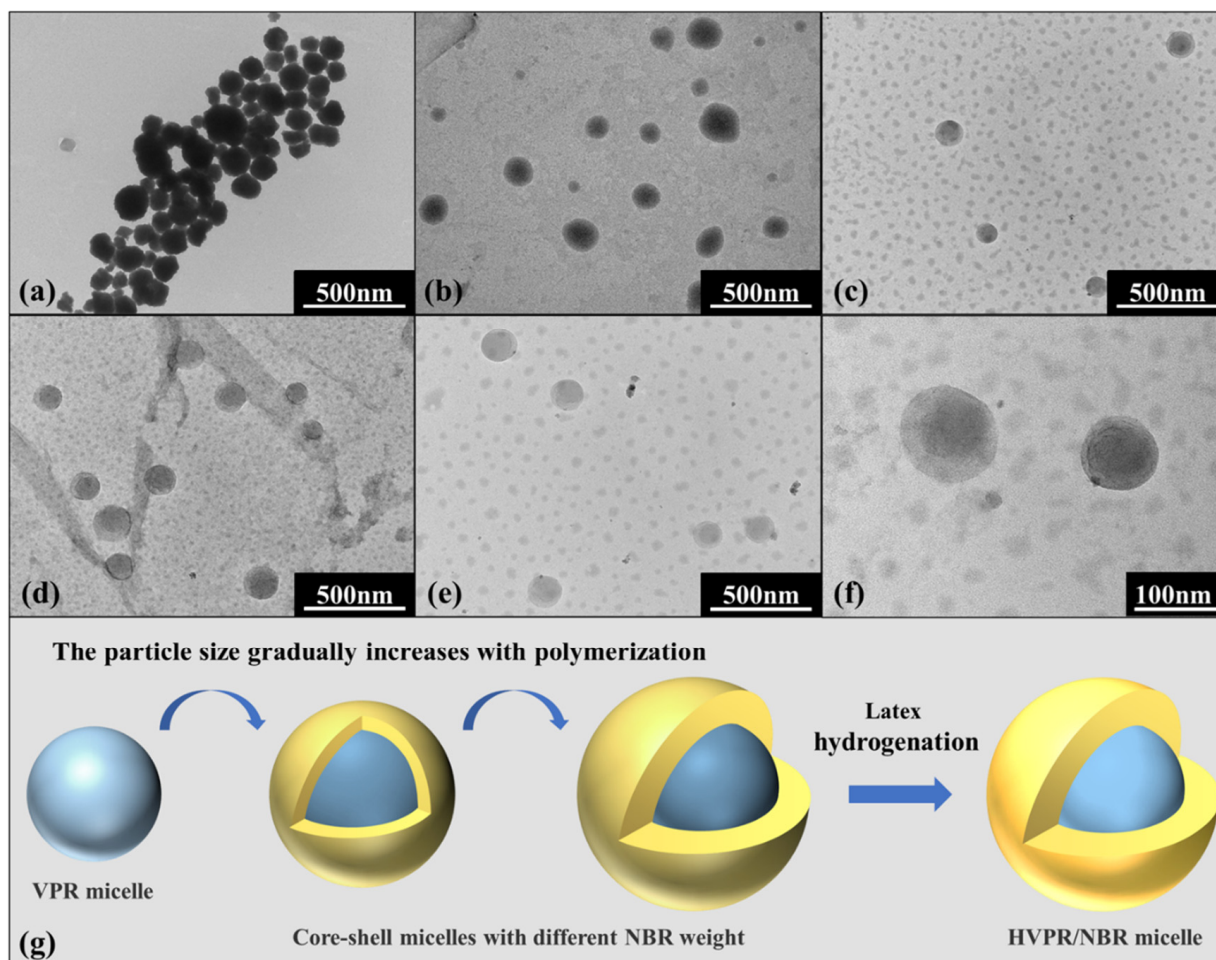


Figure 2. TEM images of VPR latex ((a): Run 1), NBR latex ((b) Run 9), VPR/NBR ((c): Run 4 and (d): Run 7) and HVPR/HNBR ((e,f): Run 14); Schematic illustration for preparation of core-shell HVPR/HNBR nanoparticles (g).

2.3. Catalytic Latex Hydrogenation of NBR Latex, VPR Latex, and VPR/NBR Core-Shell Nanoparticles Latex

Wilkinson's catalysts exhibit high catalytic activity, fast hydrogenation rate, and almost no cross-linking of hydrogenation products in the hydrogenation of unsaturated olefinic polymers, which has been demonstrated in prior studies [32–34]. In our present research, Wilkinson's catalyst was similarly employed for the homogeneous latex hydrogenation of core-shell nanoparticles. During latex hydrogenation, when multiple unsaturated groups such as C=C double bonds, aromatic rings, and cyano groups are present in the polymer, the C=C double bonds are usually preferentially reduced to single bonds, while the aromatic rings and cyano groups are retained in the process.

To assess the transformations in functional groups occurring before and after the hydrogenation of core-shell latexes, we conducted FT-IR spectroscopy on the latex samples pre- and post-hydrogenation.

The structure of the polymers was characterized by FT-IR. Figure 3a shows the FT-IR spectra of the NBR and HNBR-2 h (two hours of hydrogenation), where the peak at 2236 cm^{-1} associated with cyano ($\text{C}\equiv\text{N}$) is consistent in intensity before and after hydrogenation. This finding indicates the preservation of the integrity of the $\text{C}\equiv\text{N}$ group

during the catalytic hydrogenation process. Additional characteristic absorption peaks at 970 cm^{-1} and 917 cm^{-1} were attributed to *trans*-1,3-butadiene units and 1,2-vinyl units, respectively. After 2 h of hydrogenation, a noticeable reduction in the intensity of the absorption peak at 970 cm^{-1} was observed, while the absorption peak at 917 cm^{-1} vanished entirely. The above findings indicate that the C=C double bond on the chain of the NBR molecule is reduced to some extent. Furthermore, a new characteristic peak emerged at 723 cm^{-1} , assigned to the rocking vibration of $(\text{CH}_2)_n$ (n greater than 4). Based on these results, it is evident that hydrogenation of NBR was successfully achieved through catalytic hydrogenation, underscoring the effectiveness of this process [35,36].

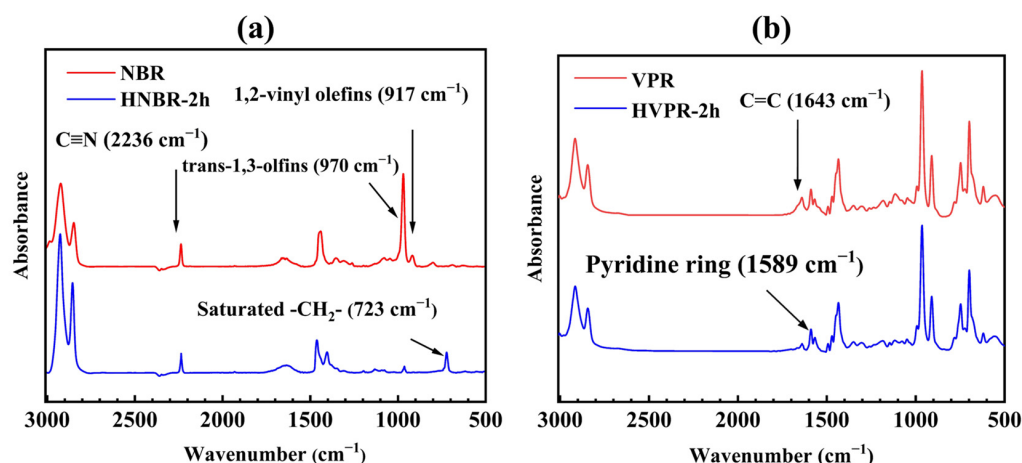


Figure 3. (a) FT-IR spectra of the original NBR and HNBR-2 h; (b) FT-IR spectra of the original VPR and HVPR-2 h.

Figure 3b presents the FT-IR spectra recorded before and after the hydrogenation of the VPR latex. The peak observed at 1643 cm^{-1} corresponded to the C=C stretching vibration present in the VPR latex. Notably, the intensity of this characteristic peak in the HVPR-2 h sample exhibited a significant decrease, which can be attributed to the reduction of unsaturated C=C bonds within the VPR molecular chains over the course of hydrogenation. This outcome serves as strong evidence for the successful hydrogenation of the VPR latex. Furthermore, the robust absorption peak associated with the pyridine ring at 1589 cm^{-1} remained unchanged. This observation confirms that the pyridine ring remained intact after hydrogenation, underscoring the effective application of Wilkinson's catalyst for the selective hydrogenation of the VPR latex.

When comparing the FT-IR spectra of the VPR or NBR with those of the core-shell nanoparticles, it becomes evident that the latter exhibit a more complex structure with more absorption peaks. Figure 4 presents the FT-IR spectra recorded before and after the hydrogenation of the VPR/NBR latex. In the core-shell nanoparticles, the absorption peak at 1643 cm^{-1} is attributed to the C=C stretching vibration of the core polymer (VPR), the intensity of which decreases with increasing hydrogenation. This decline indicates the reduction of unsaturated C=C bonds within the core portion. At the same time, the intensity of the absorption peaks of *trans*-1,3-butadiene units and 1,2-vinyl units in shell polymers is significantly decreased (occurring at 970 cm^{-1} and 917 cm^{-1} , respectively). Moreover, the absorption peaks of both unsaturated C=C double bonds decrease with the degree of hydrogenation, suggesting that the unsaturated C=C bonds in the core were simultaneously reduced. Observing the three FT-IR curves representing different hydrogenation periods in Figure 4, it is apparent that the unsaturated C=C bonds in both the core and the shell experienced a concurrent decrease to some extent during the initial stage of hydrogenation (0.5 h). As the hydrogenation process continued, the intensity of absorption peaks at 1643 cm^{-1} and 970 cm^{-1} significantly weakened after 2 h. The intensity of cyano groups on the molecular chain remained unaffected by hydrogenation in VNR/NBR latex, given these observations, the FT-IR peak corresponding to cyano

groups was selected as a reference to compare the changes in double bond characteristic peaks belonging to the molecular chains of VPR and NBR, respectively. After 0.5 h of hydrogenation treatment, the intensity of the C=C peak at 1643 cm^{-1} in the VPR molecular chain decreased by 42%, while the intensity of the peak corresponding to *trans*-1,3-butadiene units in the NBR molecular chain decreased by 43.6%. In contrast, the intensity of the newly generated peak associated with $(\text{CH}_2)_n > 4$ (at 723 cm^{-1}) increased by 44.5% compared to the levels after 99% hydrogenation. These findings suggest that there was no discernible hydrogenation sequential order within these core–shell nanoparticles. The above findings indicate that there is no barrier between the core and shell of the core–shell nanoparticles that affects hydrogen and catalyst mass transfer.

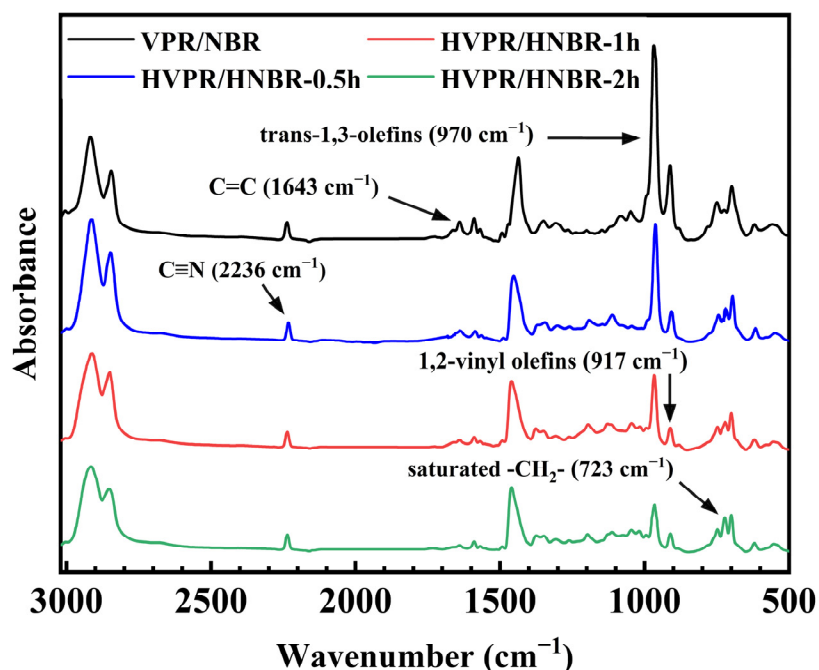


Figure 4. FT-IR spectra of VPR/NBR (black line), HVPR/HNBR-0.5 h (blue line), HVPR/HNBR-1 h (red line), and HVPR/HNBR-2 h (green line).

Based on the comprehensive findings outlined above, it is evident that the VPR/NBR latex prepared in this study underwent simultaneous hydrogenation, without a distinct sequential order. Several plausible reasons can account for this simultaneous hydrogenation phenomenon:

Effective Catalyst Dispersion: The Wilkinson’s catalyst employed in this research was well dispersed in the latex and was able to disperse thoroughly within the core–shell nanoparticles under mechanical stirring. This even distribution of the catalyst throughout the latex likely facilitated the uniform and simultaneous hydrogenation of both the core and shell polymers.

Intermittent Seeded Emulsion Polymerization: The use of the intermittent seeded emulsion polymerization method may have introduced opportunities for intricate grafting or intercalation between the core and shell layers of the nanoparticles. This enhanced compatibility between the core and shell polymers could have contributed to their synchronized hydrogenation, as the catalyst could access both polymers effectively.

These factors collectively point to a concurrent hydrogenation process in the VPR/NBR latex, highlighting the efficiency of the chosen hydrogenation method.

In our investigations, we delved into the impact of reaction temperature and catalyst mass on the hydrogenation reaction—a pivotal aspect of this study. Our findings revealed compelling insights into these factors. Firstly, we observed a substantial acceleration in the hydrogenation rate as we augmented the catalyst dosage (as depicted in Figure 5a).

Remarkably, when the catalyst dosage reached 0.05 wt%, we achieved an impressive hydrogenation degree exceeding 90% within a mere 1 h timeframe. These outcomes underscore the pivotal role of catalyst mass in driving the hydrogenation process efficiently and achieving high hydrogenation degrees.

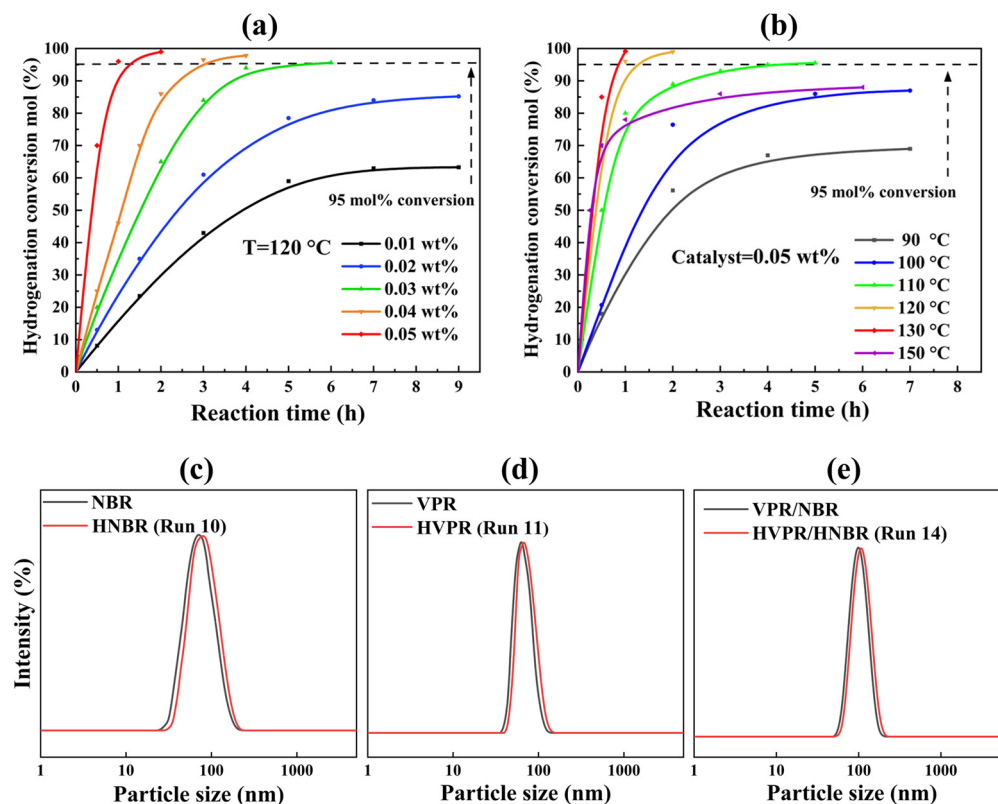


Figure 5. The effect curves of different catalyst amounts (a) and temperature (b) on the hydrogenation degree of the VPR/NBR latex; particle size distribution of NBR (c), VPR (d), and VPR/NBR (e) before and after hydrogenation for 2 h.

In the regime of chemical reactions, whether exothermic or endothermic, it is a well-established principle that reaction rates tend to increase with rising temperature. In keeping with this principle, our study unveiled a compelling trend in the hydrogenation rate of HVPR/HNBR as we raised the temperature. Notably, the hydrogenation rate exhibited a remarkable ascent, eventually surpassing the 95% hydrogenation degree range within the temperature bracket of 110 °C to 130 °C (as illustrated in Figure 5b). However, a notable deviation occurred when we elevated the temperature to 150 °C. At this juncture, the hydrogenation rate of the VPR/NBR latex exhibited a precipitous decline after a mere 0.5 h of reaction time, culminating in a hydrogenation degree of only 89% after 6 h. This decline can be attributed to deactivation of the catalyst under the harsh conditions of prolonged high-temperature reactions, resulting in the inability of the catalyst to form active centres.

2.4. Effect of Hydrogenation Process on Particle Size and Particle Size Distribution

Our investigation also encompassed an examination of how the hydrogenation process might influence the particle size distribution of different polymer latexes. Encouragingly, all three latexes, characterized by their relatively narrow particle size distribution, exhibited only slight alterations in particle size following hydrogenation (as depicted in Figure 5c–e). Furthermore, we made a noteworthy observation during this process—there were no instances of coagulation, suggesting that the core-shell nanoparticles we synthesized possessed exceptional structural stability. This stability held true even when subjected to the demanding conditions of high temperature and H₂ pressure hydrogenation.

3. Materials and Methods

3.1. Materials

VPR (solid content = 41.25%) was purchased from LANXESS (Pittsburgh, PA, USA). Acrylonitrile (ACN, 99%), methyl ethyl ketone (MEK, reagent grade), ethanol (reagent grade), and acetone (reagent grade) were all purchased from Aladdin Reagent (Shanghai, China) Co., Ltd. Ammonium persulfate (APS, 98%), *tert*-dodecylmercaptan (*t*-DDM, 99%), *N,N*-diethylhydroxylamine (DEHA, 98%), and sodium dodecyl sulfate (SDS, 99%) were purchased from Sigma-Aldrich (St. Louis, MO, USA). Nitrogen (N₂, 99.99%), and 1,3-butadiene (BD, 99%) was purchased from Qingdao Ludong Gas Co., Ltd., Qingdao, China.

The distilled water used in the experiments was self-made in the laboratory. The inhibitors were removed prior to polymerization by passing the monomer ACN through an alumina column.

3.2. Methods

3.2.1. Polymerization

- VPR/NBR Seeded Emulsion Polymerization

The seeded emulsion polymerization of VPR/NBR was conducted in a Parr 316 stainless steel reactor. Detailed polymerization conditions and product characterizations are summarized in Table 1 (Runs 2–8). The typical polymerization procedure is outlined below:

Table 1. Polymerization recipe and experimental results for the synthesis of VPR/NBR core-shell nanoparticle latex and NBR nanoparticle latex.

Run ^(a)	Water ^(b) (wt%)	Weight of VPR (g)	Weight of NBR ^(c) (g)	Temperature (°C)	Dz (nm)	$N_p \times 10^{19}$ ^(d)	PDI
1	–	60	0	–	86.7	1.17	0.045
2	46.3	30	15	50	98.5	1.21	0.043
3	46.3	30	15	60	97.3	1.22	0.046
4	46.3	30	15	70	94.4	1.27	0.047
5	81.3	30	30	70	99.6	1.29	0.042
6	116.3	30	45	70	103.1	1.36	0.039
7	151.3	30	60	70	106.3	1.39	0.041
8	46.3	30	15	80	94.6	1.25	0.045
9	140	0	60	70	91.3	1.13	0.40

^(a) Polymerization conditions of VPR/NBR and NBR was as follow: solid content of VPR = 41.25%, Acrylonitrile content of NBR = 36%, APS = 0.1 wt%, SDS = 3.5 wt%, *t*-DDM = 0.3 wt%, DEHA = 0.2 wt%, and stirring rate = 350 rpm. ^(b) Distilled water was added to ensure that the solids content of latex was controlled at 30 ± 2%. ^(c) Weight of NBR was the mass of NBR on polymer in latex at 80% conversion rate. ^(d) The number of polymer particles (N_p) was calculated according to Equation (1).

APS, SDS, and *t*-DDM were initially dissolved in distilled water and stirred at room temperature until a homogeneous solution was formed. This solution was then added to the reactor.

The seed latex (VPR latex) was added to the reactor, and the resulting mixture was degassed with three quick cycles of N₂ (99.99%) and subjected to bubbling N₂ at approximately 0.5 MPa for 30 min at room temperature, with a stirring rate of 160 rpm.

The system was slowly heated to the desired reaction temperature (50, 60, 70, or 80 °C), while maintaining a stirring rate of 350 rpm. After the temperature stabilized for 0.5 h, a mixture of ACN and BD was added to the reactor.

Following the addition of monomers, the polymerization system was allowed to age for an additional 2–4 h to achieve the desired polymer conversion.

Latex samples were withdrawn from a dip tube at hourly intervals to calculate the conversion rate using Equation (2), as mentioned later in the manuscript.

The reaction was halted by rapidly immersing the reactor vessel in an ice bath to arrest polymerization. Short-stopper DEHA was added.

The VPR/NBR latex underwent hydrogenation experiments after post-treatment, including the removal of monomers [37].

- NBR Emulsion Polymerization

The NBR latex was utilized for the preparation of HNBR in contrast to the hydrogenated VPR/NBR core-shell latex. Detailed polymerization conditions and latex characterization are presented in Table 1 (Run 9). The experimental process closely resembled the typical polymerization procedure outlined earlier, with the exception that the NBR polymerization experiment did not involve the addition of seed latex.

$$N_p = 6MX_f / (\pi\rho_p D_v^3) \quad (1)$$

where N_p is the number of latex particles per unit volume of water; M is the mass of monomer per unit volume of water; ρ_p is the density of polymer; D_v is the average particle size; X_f is the polymerization conversion of mixed monomers.

The synthesized core-shell latex, consisting of poly(butadiene-styrene-vinyl pyridine)/poly(acrylonitrile-butadiene), was abbreviated as VPR/NBR. Additionally, pure VPR latex without a core-shell structure (refer to Run 1 in Table 1) was obtained for comparative purposes with the VPR/NBR latex and for subsequent HVPR preparation in hydrogenation experiments.

3.2.2. Post-Processing of Polymer Latex

The core-shell latex obtained previously contained residual monomers with some level of toxicity and an irritating odor, which could potentially impact the catalytic activity of the catalysts during the subsequent hydrogenation process. To address this, a devolatilization method was employed to eliminate these residual monomers from the latex.

The devolatilization process involved distilling the latex under vacuum conditions at 45 °C for a duration of 40 min, maintaining a pressure of 40 mbar. This step effectively removed the butadiene (BD) monomers along with a portion of the acrylonitrile (ACN). Subsequently, the remaining ACN was removed through a steam distillation process conducted at 70 °C.

3.2.3. Hydrogenation

- VPR/NBR Core-shell Latex Hydrogenation

The catalytic hydrogenation of the VPR/NBR core-shell latex was conducted in the same reactor. The detailed polymerization conditions and hydrogenation degrees of the latex are summarized in Table 2, which will be presented later in this study. The following outlines a typical procedure for latex hydrogenation:

Table 2. Hydrogenation conditions of VPR, NBR, and core-shell VPR/NBR polymers.

Run	Latex	Wilkinson's Catalyst (wt%)	SDS (wt%)	Time (h)	Temperature (°C)	Pressure (MPa)	Hydrogenation Degree (%)
10	NBR	0.025	3	2	120	8.6	92.8
11	VPR	0.025	3	2	120	8.6	88.6
12	VPR/NBR	0.04	3	0.5	120	8.6	28.6
13	VPR/NBR	0.04	3	1	120	8.6	58.5
14	VPR/NBR	0.04	3	2	120	8.6	85.3

A measured volume of the VPR/NBR core–shell latex (60 g) was combined with distilled water (90 g) and a specific amount of Wilkinson’s catalyst. The mixture in the reactor was degassed by subjecting it to three quick cycles of nitrogen (N₂) and then bubbling N₂ at approximately 0.5 MPa for 30 min at room temperature, with a stirring rate of 160 rpm. The reactor was gradually heated to the reaction temperature (120 °C) while maintaining a stirring rate of 450 rpm, and this temperature was held for 30 min. The hydrogenation reaction commenced when hydrogen gas at a pressure of 8.6 MPa was introduced into the reactor. The conditions of hydrogen pressure (8.6 MPa), hydrogenation temperature (120 °C), and stirring rate (450 rpm) were maintained consistently throughout the entire reaction duration. Aliquots were collected at intervals of 0.5, 1, and 2 h using a dip tube. Finally, the system was depressurized to obtain the final latex after cooling to room temperature.

- NBR Latex Hydrogenation without Seed

The NBR latex obtained from the emulsion polymerization experiments mentioned earlier was employed to produce HNBR latex. To investigate the hydrogenation sequence of VPR/NBR core–shell nanoparticles, Fourier Transform Infrared (FT–IR) spectra of pure NBR latex were recorded. Detailed information regarding the hydrogenation conditions and degree for the latex is summarized in Table 2 (Run 10). The hydrogenation process of the NBR latex closely resembled the typical hydrogenation procedure described above, with the exception of the catalyst dosage, which was set at 0.025 wt% for the NBR latex hydrogenation experiment. HNBR data were collected after a 2 h hydrogenation period for comparison purposes.

- VPR Latex Hydrogenation without Shell

The commercially purchased VPR latex was diluted with distilled water and subsequently subjected to hydrogenation. Comprehensive information regarding the hydrogenation conditions and degree for this latex is outlined in Table 2 (Run 11).

To gain insights into alterations in characteristic groups during the hydrogenation of VPR/NBR core–shell nanoparticles, control experiments involving the hydrogenation of NBR and VPR latex were devised. The hydrogenation process for the VPR latex mirrored that of the NBR latex.

3.3. Characterization

3.3.1. Particle Size

The intensity-based particle size distribution, particle dispersibility index (PDI), and Z-average particle size of the core and core–shell latex nanoparticles were determined by DLS (Zetasizer Nano ZS, Malvern Instruments, Worcestershire, UK) at 25 °C. The particle size measurements of samples were respectively tested parallel three times and averaged [38].

3.3.2. Transmission Electron Microscope (TEM)

The morphology of core–shell nanoparticles was observed by LEO 912 AB 100 kV Energy Filtered Transmission Electron Microscope (EFTEM) (Carl Zeiss AG, Jena, Germany). The preparation process for TEM measurements was as follows: the nanosized latex was firstly diluted with distilled water, and 10 µL of the obtained diluted solution was placed on a 400-mesh copper grid at room temperature. Next, the grid was negatively stained with 2% (*w/v*) phosphotungstic acid for 1 min. After removing the excess stain, the grid was placed in a TEM chamber for imaging [39].

3.3.3. Fourier Transform Infrared Spectrometer (FT–IR) and Attenuated Total Reflectance (ATR)

The FT–IR spectra were recorded on a Bruker tensor II infrared spectrograph (Bruker tensor II, Karlsruhe, Germany). The ATR technology was one of the infrared spectral analysis methods to measure the absorption spectra of solids and liquids. A typical method for preparing polymer solids and analyzing by the ATR technology is presented below.

The latex was firstly dropped into ethanol to obtain the polymer solid. The solid was then washed with ethanol and distilled water successively at the stirring speed of 160 rpm and dried under vacuum at 45 °C overnight. The obtained purified polymer solid was analyzed by the ATR technology. For the FT-IR analysis, the total reflectance crystal was mounted on a holder, while the solid rubber was placed on the reflective surface of the total reflectance crystal.

3.3.4. Conversion Rate of Polymerization

The conversion rate of the monomers (BD and ACN) was calculated using the mass method. The conversion rate at instant time t could be defined as the ratio of the mass of the newly formed polymer in the reactor at time t (m_t) to the mass of the monomer added before the start of the polymerization (m_0). As shown in Equation (2)

$$\alpha = \frac{m_t}{m_0} \quad (2)$$

The solid mass of the surfactant and seed latex was identified as a constant. The solid mass of the sample at t was measured using a Halogen Moisture Analyzer (METTLER TOLEDO HX204, Zurich, Switzerland), based on which the polymerization conversion rate of the VPR/NBR latex was calculated according to Equation (3).

$$\alpha = \frac{SD - (m_1 + m_2)/M}{m_0/M} \quad (3)$$

where SD is the solid content measured by a moisture meter, m_1 is the solid content of the seed latex VPR, m_2 is the mass of the surfactant used in the polymerization, M is the total mass of solid in the system under complete monomer reaction.

3.3.5. Hydrogenation Degree

The hydrogenation degree of the VPR/NBR core-shell latex, NBR latex, and VPR latex was calculated using the iodine value titration method according to SH/T 1763-2008 [40]. Specifically, 9 g of iodine and 8 g of iodine chloride were first dissolved in 1 L of acetic acid to obtain Wijs reagent (purple color). And 1–2 g of solid gum sample was dissolved in chloroform to obtain a rubber solution. Then, the Wijs reagent was added into the rubber solution. After aging for 2 h, 10 mL of potassium iodide solution (20%), 100 mL of distilled water, and 6 mL of starch solution were added to the above solution. Finally, the solution was titrated with sodium thiosulfate solution (0.05 mol/L): the amount of sodium thiosulfate solution was recorded when the color of the solution became transparent.

$$\text{Iodine number} = \frac{0.1269 \times (V_0 - V \times 0.05)}{m \times 100} \quad (4)$$

where V_0 is the volume of sodium thiosulfate consumed in the blank experiment; V is the volume of sodium thiosulfate consumed in the titration sample; m is the mass of the sample.

4. Conclusions

In this study, core-shell nanoparticles with VPR as the core and NBR as the shell were successfully prepared by seed emulsion polymerization. The particle size of the core-shell nanoparticles increased from 86 nm to 105 nm after the introduction of NBR shell and maintained a uniform particle size distribution. The effects of polymerization temperature and monomer mass on the size and number of particles (N_p) of the core-shell nanoparticles were investigated, and it is noteworthy that higher polymerization temperatures favored the formation of more nanoparticles, but the number of particles decreased instead when the temperature was increased to 80 °C. In addition, we obtained the hydrogenation product HVPR/HNBR by direct catalytic hydrogenation of core-shell latex using Wilkinson's catalyst, and systematically investigated the effects of catalyst

dosage and reaction temperature on the hydrogenation reaction of core-shell nanoparticles in latex. The results showed that increasing the catalyst dosage could effectively improve the hydrogenation rate, and the degree of hydrogenation of latex reached 95 mol% in 2 h when the catalyst dosage was 0.05 wt%. Increasing the reaction temperature effectively improved the hydrogenation rate, and the fastest hydrogenation rate was achieved at 130 °C, but when the temperature was increased to 150 °C, the rate of hydrogenation was reduced instead, and the final degree of hydrogenation of latex was less than 90 mol%. By analyzing the FT-IR spectra of the core-shell nanoparticles HVPR/HNBR, we investigated the hydrogenation sequence of the two polymers in the core-shell particles, and it is noteworthy that the hydrogenation processes of the core (VPR) and the shell (NBR) were carried out almost simultaneously, and the stability of the latex was maintained throughout the whole hydrogenation process. In this study, the hydrogenation of a special core-shell structure nanoparticle in latex is realized, which provides a new idea and direction for the green emulsion hydrogenation technology.

Author Contributions: Conceptualization, F.Y., Y.J. and H.W.; methodology, F.Y. and H.W.; validation, F.Y., X.L. and H.W.; formal analysis, J.D. and B.Z.; investigation, F.Y. and X.S.; resources, H.W., Y.L. and Y.J.; data curation, F.Y. and L.L.; writing—original draft preparation, F.Y.; writing—review and editing, F.Y., X.L., Y.J. and J.L.; visualization, Y.L., L.L. and H.W.; supervision, H.W.; funding acquisition, H.W. All authors have read and agreed to the published version of the manuscript.

Funding: This work was supported by the Key Research and Development Program of Jiangsu Province (grant numbers BE2021070); the Taishan Scholar Project of Shandong Province (grant numbers ts201712047) and the Natural Science Foundation of Shandong Province (grant numbers ZR2019MB001).

Data Availability Statement: All data generated or analyzed during this study are included in this published article.

Conflicts of Interest: Author Yigao Jiang was employed by the Yangzhou High-Tech Rubber & Plastic Limited Company. The remaining authors declare that the research was conducted in the absence of any commercial or financial relationships that could be construed as a potential conflict of interest.

References

1. Lovell, P.A.; Schork, F.J. Fundamentals of Emulsion Polymerization. *Biomacromolecules* **2020**, *21*, 4396–4441. [[CrossRef](#)] [[PubMed](#)]
2. Qi, Y.; Liu, Z.; Liu, S.; Cui, L.; Dai, Q.; He, J.; Dong, W.; Bai, C. Synthesis of 1,3-Butadiene and Its 2-Substituted Monomers for Synthetic Rubbers. *Catalysts* **2019**, *9*, 97. [[CrossRef](#)]
3. Visseaux, M. Catalysts for the Controlled Polymerization of Conjugated Dienes. *Catalysts* **2018**, *8*, 442. [[CrossRef](#)]
4. Hlalele, L.; D'hooge, D.R.; Dürr, C.J.; Kaiser, A.; Brandau, S.; Barner-Kowollik, C. RAFT Mediated ab Initio Emulsion Copolymerization of 1,3-Butadiene with Acrylonitrile. *Macromolecules* **2014**, *47*, 2820–2829. [[CrossRef](#)]
5. Kausar, A. Emulsion polymer derived nanocomposite: A review on design and tailored attributes. *Polym. Plast. Technol. Mater.* **2022**, *59*, 1737–1750. [[CrossRef](#)]
6. Chern, C.S. Emulsion polymerization mechanisms and kinetics. *Prog. Polym. Sci.* **2006**, *31*, 443–486. [[CrossRef](#)]
7. Chen, L.; Hong, L.; Lin, J.; Meyers, G.; Harris, J.; Radler, M. Epoxy-acrylic core-shell particles by seeded emulsion polymerization. *J. Colloid Interface Sci.* **2016**, *473*, 182–189. [[CrossRef](#)] [[PubMed](#)]
8. Wang, L.; Ion, F.; Petrescu, T.; Liu, J.; Li, H.; Shi, G. Synthesis of Dimpled Particles by Seeded Emulsion Polymerization and Their Application in Superhydrophobic Coatings. *Membranes* **2022**, *12*, 876. [[CrossRef](#)]
9. Wang, H.; Pan, Q.; Hammond, M.; Rempel, G.L. Preparation of Poly(methyl methacrylate)-Poly(acrylonitrile-co-butadiene) Core-Shell Nanoparticles. *J. Polym. Sci. Part A Polym. Chem.* **2012**, *50*, 736–749. [[CrossRef](#)]
10. Sheng, X.; Xie, D.; Yang, W.; Zhang, X.; Zhong, L. High solid content poly(butyl acrylate)/poly(methyl methacrylate) core/shell nanosized spheres synthesised by microemulsion polymerization. *Micro Nano Lett.* **2016**, *11*, 164–168. [[CrossRef](#)]
11. Mun, H.; Hwang, K.; Kim, W. Synthesis of emulsion styrene butadiene rubber by reversible addition-fragmentation chain transfer polymerization and its properties. *J. Appl. Polym. Sci.* **2019**, *136*, 47069. [[CrossRef](#)]
12. Giurginca, M.; Zaharescu, T. Thermal and radiation behaviour of HNBR and CSPE blends. *Polymer* **2000**, *41*, 7583–7587. [[CrossRef](#)]
13. Tong, W.; Chen, H.; Zhang, Y.; Zhang, Z.; Fu, Y.; Qi, H.; Zhou, D.; Li, Y.; Wang, H. Selective hydrogenation of nitrile butadiene rubber latex using Catmetium®RF 4 catalyst. *Catal. Today* **2023**, *407*, 80–88. [[CrossRef](#)]
14. Guerriero, A.; Peruzzini, M.; Gonsalvi, L. Ruthenium (II)-Arene Complexes of the Water-Soluble Ligand CAP as Catalysts for Homogeneous Transfer Hydrogenations in Aqueous Phase. *Catalysts* **2018**, *8*, 88. [[CrossRef](#)]

15. Schulz, G.A.S.; Comin, E.; de Souza, R.F. Catalytic hydrogenation of nitrile rubber using palladium and ruthenium complexes. *J. Appl. Polym. Sci.* **2007**, *106*, 659–663. [[CrossRef](#)]
16. Yue, D.M.; Shen, Z.M.; Xu, R.Q.; Wei, Y.K. A New Bimetallic Complex Catalyst for NBR Hydrogenation and Properties of Hydrogenated NBR. *J. Elastomers. Plast.* **2016**, *34*, 225–237. [[CrossRef](#)]
17. Wang, X.; Sun, J.; Wang, C.; Zong, C. Diimide hydrogenation of NBR latex using different zinc ions catalytic system. *Colloid. Polym. Sci.* **2022**, *300*, 661–674. [[CrossRef](#)]
18. Samran, J.; Phinyocheep, P.; Daniel, P.; Kittipoom, S. Hydrogenation of unsaturated rubbers using diimide as a reducing agent. *J. Appl. Polym. Sci.* **2005**, *95*, 16–27. [[CrossRef](#)]
19. Wang, H.; Yang, L.; Rempel, G.L. Homogeneous Hydrogenation Art of Nitrile Butadiene Rubber: A Review. *Polym. Rev.* **2013**, *53*, 192–239. [[CrossRef](#)]
20. Liu, X.; Fu, Y.; Zhou, D.; Chen, H.; Li, Y.; Song, J.; Zhang, S.; Wang, H. Hydrogenation of Carboxyl Nitrile Butadiene Rubber Latex Using a Ruthenium-Based Catalyst. *Catalysts* **2022**, *12*, 97. [[CrossRef](#)]
21. Cao, P.; Huang, C.; Zhang, L.; Yue, D. One-step fabrication of RGO/HNBR composites via selective hydrogenation of NBR with graphene-based catalyst. *RSC Adv.* **2015**, *5*, 41098–41102. [[CrossRef](#)]
22. Lin, X.; Pan, Q.; Rempel, G.L. Hydrogenation of nitrile-butadiene rubber latex with diimide. *Appl. Catal. A Gen.* **2004**, *276*, 123–128. [[CrossRef](#)]
23. Ai, C.; Gong, G.; Zhao, X.; Liu, P. Selectively Catalytic Hydrogenation of Nitrile-Butadiene Rubber Using Grubbs II Catalyst. *Macromol. Res.* **2017**, *25*, 461–465. [[CrossRef](#)]
24. Wang, H.; Pan, Q.; Rempel, G.L. Diene-Based Polymer Nanoparticles: Preparation and Direct Catalytic Latex Hydrogenation. *J. Polym. Sci. Part A Polym. Chem.* **2012**, *50*, 2098–2110. [[CrossRef](#)]
25. Lamb, D.J.; Fellows, C.M.; Gilbert, R.G. Radical entry mechanisms in redox-initiated emulsion polymerizations. *Polymer* **2005**, *46*, 7874–7895. [[CrossRef](#)]
26. Thickett, S.C.; Gilbert, R.G. Emulsion polymerization: State of the art in kinetics and mechanisms. *Polymer* **2007**, *48*, 6965–6991. [[CrossRef](#)]
27. Joseph Schork, F. Monomer transport in emulsion polymerization. *Can. J. Chem. Eng.* **2022**, *100*, 645–653. [[CrossRef](#)]
28. Wang, H.; Rempel, G.L. Organic solvent-free catalytic hydrogenation of diene-based polymer nanoparticles in latex form: Mass transfer of hydrogen in a semibatch process. *J. Ind. Eng. Chem.* **2015**, *25*, 29–34. [[CrossRef](#)]
29. de Arbina, L.L.; Barandiaran, M.J.; Gugliotta, L.M.; Asuat, J.M. Emulsion polymerization: Particle growth kinetics. *Polymer* **1996**, *37*, 5907–5916. [[CrossRef](#)]
30. Wang, Y.; Cao, F.; Fu, Y.; Chen, H.; Zhang, Y.; Wang, C.; Li, Y.; Wang, H. Preparation of Diene-based Nanoparticles by Semibatch Microemulsion Polymerization and Their Catalytic Hydrogenation. *Catal. Today* **2023**, *407*, 156–164. [[CrossRef](#)]
31. Kuwano, N.; Kaur, J.; Rahmah, S. Electron microscopy determination of crystallographic polarity of aluminum nitride thin films. *Micron* **2019**, *116*, 80–83. [[CrossRef](#)] [[PubMed](#)]
32. Wei, Z.; Wu, J.; Pan, Q.; Rempel, G.L. Direct Catalytic Hydrogenation of an Acrylonitrile-Butadiene Rubber Latex Using Wilkinson's Catalyst. *Macromol. Rapid Commun.* **2005**, *26*, 1768–1772. [[CrossRef](#)]
33. Nelson, D.; Li, R. Christopher Brammer. Using Correlations to Compare Additions to Alkenes: Homogeneous Hydrogenation by Using Wilkinson's Catalyst. *J. Org. Chem.* **2005**, *70*, 761–767. [[CrossRef](#)] [[PubMed](#)]
34. Matsubara, T.; Takahashi, R.; Asai, S. ONIOM Study of the Mechanism of Olefin Hydrogenation by the Wilkinson's Catalyst: Reaction Paths and Energy Surfaces of trans- and cis-Forms. *Bull. Chem. Soc. Jpn.* **2013**, *86*, 243–254. [[CrossRef](#)]
35. Brück, D. IR spectrometric determination of the proportions of acrylonitrile, butadiene and hydrogenated butadiene in hydrogenated acrylonitrile-butadiene rubbers. Part 1. Principles. *Kautsch. Gummi Kunstst.* **1989**, *42*, 107–110.
36. Brück, D. IR spectrometric determination of the proportions of acrylonitrile, butadiene and hydrogenated butadiene in hydrogenated acrylonitrile-butadiene rubbers. Part 2. Residual double bonds in commercial HNBR products. *Kautsch. Gummi Kunstst.* **1989**, *42*, 194–197.
37. Wang, H.; Chan, E.; Bregu, S.; Rempel, G.L. Preparation of Poly(styrene-co-butadiene) Fine Latex via a Gemini Surfactant Induced Low Temperature Initiation Semibatch Emulsion Polymerization System. *J. Polym. Sci. Part A Polym. Chem.* **2016**, *54*, 1669–1678. [[CrossRef](#)]
38. Zhang, S.; Zhang, Q.; Shang, J.; Mao, Z.; Yang, C. Measurement methods of particle size distribution in emulsion polymerization. *Chin. J. Chem. Eng.* **2021**, *39*, 1–15. [[CrossRef](#)]
39. Chen, S.A.; Lee, S.T. Seeded latex polymerizations: Studies on the particle growth mechanism of latex particles. *Polymer* **1992**, *33*, 1437–1444. [[CrossRef](#)]
40. SH/T 1763-2008; Nitrile Rubber. Determination of Residual Unsaturation in Hydrogenated Nitrile Rubber (HNBR) by Iodine Value. The Standardization Administration of the People's Republic of China: Beijing, China, 2008.

Disclaimer/Publisher's Note: The statements, opinions and data contained in all publications are solely those of the individual author(s) and contributor(s) and not of MDPI and/or the editor(s). MDPI and/or the editor(s) disclaim responsibility for any injury to people or property resulting from any ideas, methods, instructions or products referred to in the content.